

CMS-B2G-25-003

CERN-EP-2025-270  
2026/01/21

# Combination of searches for heavy vector boson resonances in proton-proton collisions at $\sqrt{s} = 13$ TeV

The CMS Collaboration

## Abstract

A combined statistical analysis of searches for heavy vector boson resonances decaying into pairs of  $W$ ,  $Z$ , or Higgs bosons, as well as into quark pairs ( $q\bar{q}$ ,  $b\bar{b}$ ,  $t\bar{t}$ ,  $t\bar{b}$ ) or lepton pairs ( $\ell^+\ell^-$ ,  $\ell\bar{\nu}$ ), with  $\ell = e, \mu, \tau$ , is presented. The results are based on proton-proton collision data at a center-of-mass energy of 13 TeV, corresponding to an integrated luminosity of  $138\text{ fb}^{-1}$ , collected by the CMS experiment from 2016 to 2018. No significant deviation from the expectations of the standard model is observed. The results are interpreted in the simplified heavy vector triplet (HVT) framework, setting 95% confidence level upper limits on the production cross sections and coupling strengths to standard model particles or the HVT bosons. The results exclude HVT resonances with masses below 5.5 TeV in a weakly coupled scenario, below 4.8 TeV in a strongly coupled scenario, and up to 2.0 TeV in the case of production via vector boson fusion. The combination provides the most stringent constraints to date on new phenomena predicted by the HVT model.

*Submitted to the Journal of High Energy Physics*



## 1 Introduction

Over the past half century, searches at particle colliders for heavy resonances decaying into two-body final states have led to several discoveries. For example, the discovery of the  $W$  and  $Z$  bosons in the 1980s through their leptonic decay channels provided critical evidence compatible with the standard model (SM) [1–4] predictions. More recently, the observation of the Higgs ( $H$ ) boson in 2012, decaying into both bosonic and fermionic channels, confirmed the electroweak symmetry breaking mechanism [5–7].

The search for heavy resonances is a central component of the physics program at the CERN LHC, aiming to uncover physics beyond the SM (BSM) across a wide range of final states [8–11]. Among the theorized BSM resonances, the spin-1 heavy partners of the  $W$  and  $Z$  bosons are named  $W'$  and  $Z'$ , respectively, and are collectively referred to as  $V'$ . At the LHC, both the ATLAS and CMS Collaborations have conducted extensive searches for  $V'$  bosons that couple to SM particles via electroweak interactions [10–12]. These analyses search for the decay of a  $V'$  boson into two massive SM bosons ( $W$ ,  $Z$ , or  $H$ ), two leptons, or two quarks.

Depending on the underlying model, these heavy resonances could couple predominantly to SM fermions, as predicted by minimal  $W'$  and  $Z'$  models [13, 14], or to SM bosons, as proposed in scenarios such as composite Higgs or little Higgs models [15–17]. In some cases, these resonances could act as a bridge, or portal, between SM and dark-matter particles, providing experimental access to otherwise undetectable particles in the dark sector [18]. The heavy vector triplet (HVT) framework [19] provides a general parameterization for the production and decay of heavy spin-1 resonances that couple to quarks, leptons, vector bosons, and  $H$  bosons. Depending on the specific choice of the model parameters, the dominant production mechanism for a  $V'$  boson at the LHC can be either quark-antiquark annihilation through the Drell–Yan (DY) process, or vector boson fusion (VBF). Representative Feynman diagrams for both production mechanisms and subsequent HVT boson decays are shown in Fig. 1.

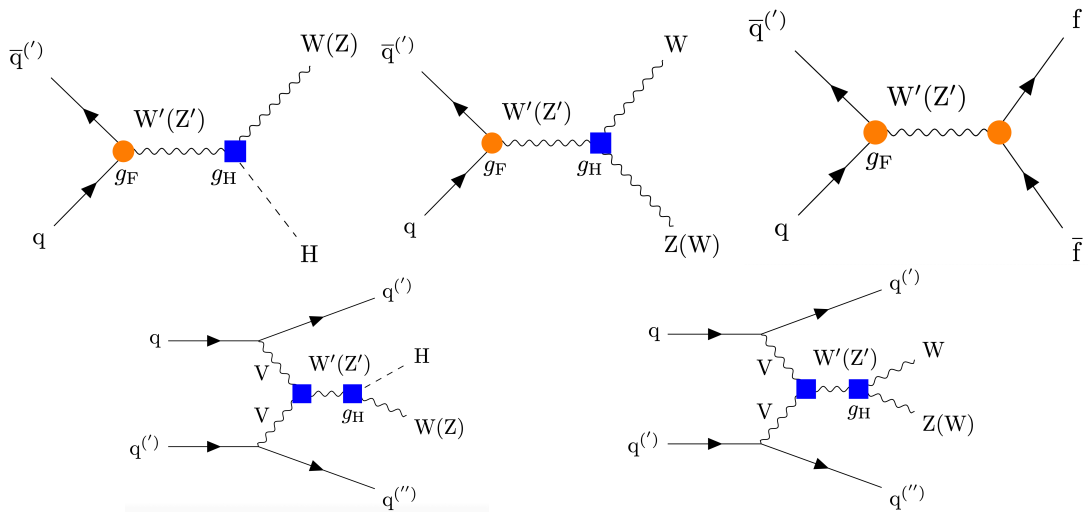


Figure 1: Representative Feynman diagrams for the production and decay of  $W'$  and  $Z'$  bosons via the Drell–Yan process (upper row) and the VBF process (lower row). The  $W'$  ( $Z'$ ) boson decays to  $WH$  ( $ZH$ ) (upper left, lower left),  $WZ$  ( $WW$ ) (upper middle, lower right), and fermion-antifermion pairs (upper right). The orange circle and the blue square indicate the fermionic and bosonic interaction vertices, respectively. The definition of the couplings is provided in Section 3.

This paper presents a combined statistical analysis of CMS searches for heavy spin-1 resonances

decaying into pairs of bosons or fermions, interpreted in the context of the HVT framework. A combined analysis of multiple channels is essential to maximize the sensitivity and fully exploit the outcome of these searches, particularly in light of localized excesses of events observed in individual channels. For instance, a combined search by the CMS Collaboration for heavy resonance decays to WW, WZ, ZZ, WH, or ZH in the fully hadronic final states [20], based on a data sample of proton-proton (pp) collisions at a center-of-mass energy of 13 TeV, corresponding to an integrated luminosity of  $138 \text{ fb}^{-1}$ , reported two excesses of events, each with a local significance of 3.6 standard deviations (SD), at 2.1 and 2.9 TeV. Similarly, in a combination of spin-1 resonance analyses using pp collision data at the same center-of-mass energy, corresponding to an integrated luminosity of  $139 \text{ fb}^{-1}$ , the ATLAS Collaboration observed a local excess over the background prediction of 2.6 SD at 1.5 TeV [11]. While these deviations are not statistically significant enough to claim evidence for BSM physics, a combined interpretation including different analyses and final states often improves the sensitivity of the search, providing a more robust assessment of potential deviations from the SM expectations.

The results presented here improve upon the previous CMS combination based on the 2016 data set [10] and provide the most stringent constraints to date on BSM scenarios involving a triplet of heavy vector boson resonances. These results represent a significant improvement over previous constraints from similar statistical combinations, driven by the inclusion of a larger data set and advances in the underlying analyses. All input analyses are based on the 2016–2018 data set, corresponding to an integrated luminosity of  $138 \text{ fb}^{-1}$  of pp collisions at a center-of-mass energy of 13 TeV. The combination includes the most sensitive channels for spin-1 resonance decays, including WW, WZ, WH, ZH, and various fermion pairs such as  $q\bar{q}$ ,  $bb$ ,  $t\bar{t}$ ,  $t\bar{b}$ ,  $\ell^+\ell^-$ , and  $\ell\bar{\nu}$ , where  $\ell = e, \mu, \tau$ . Charge-conjugate states are implied throughout the paper. The tabulated results are provided in a HEPData record [21].

## 2 The CMS detector and event reconstruction

The central feature of the CMS apparatus is a superconducting solenoid of 6 m internal diameter, providing a magnetic field of 3.8 T. Within the solenoid volume are a silicon pixel and strip tracker, a lead tungstate crystal electromagnetic calorimeter, and a brass and scintillator hadron calorimeter, each composed of a barrel and two endcap sections. Forward calorimeters extend the pseudorapidity coverage provided by the barrel and endcap detectors. Muons are measured in gas-ionization detectors embedded in the steel flux-return yoke outside the solenoid. More detailed descriptions of the CMS detector are provided in Refs. [22, 23].

Events of interest are selected using a two-tiered trigger system [24]. The first level (L1), composed of custom hardware processors, uses information from the calorimeters and muon detectors to select events at a rate of approximately 100 kHz with a fixed latency of about  $4 \mu\text{s}$  [25]. The second level, known as the high-level trigger, consists of a farm of processors running a version of the full event reconstruction software optimized for fast processing, and reduces the event rate to a few kHz before data storage [24, 26].

A particle-flow (PF) algorithm [27] aims to reconstruct and identify each individual particle (photon, electron, muon, and charged and neutral hadron) in an event, with an optimized combination of information from the various elements of the CMS detector. For each event, hadronic jets are clustered from these reconstructed particles using the infrared and collinear safe anti- $k_T$  algorithm [28, 29]. Small- and large-radius jets are clustered with distance parameters of  $R = 0.4$  and  $R = 0.8$ , respectively. Jet momentum is determined as the vectorial sum of all particle momenta in the jet, and is found from simulation to be, on average, within 5 to 10%

of the true momentum over the entire  $p_T$  spectrum and detector acceptance.

Additional pp interactions within the same or nearby bunch crossings (pileup) can contribute additional tracks and calorimetric energy depositions, increasing the jet momentum. Pileup effects are mitigated using dedicated algorithms such as the charged-hadron subtraction and the pileup-per-particle identification (PUPPI) methods [30, 31]. The PUPPI algorithm is applied to reduce the pileup dependence of the  $\vec{p}_T^{\text{miss}}$  observable, by weighting particle momenta according to their probability of originating from the primary interaction vertex [32].

Jet energy corrections are derived from simulation studies so that the average measured energy of jets becomes identical to that of jets at the particle level. In situ measurements of the momentum balance in dijet,  $\gamma$ -jets,  $Z$ -jets, and multijet events are used to determine any residual differences between the jet energy scale in data and simulation, and appropriate corrections are made [33]. Additional selection criteria are applied to each jet to remove jets originating from instrumental effects or reconstruction failures [31].

For small-radius jets, neural-network-based taggers calibrated using collision data are used to identify jets originating from the hadronization of b quarks (b tagging) [34–36]. For large-radius jets, the soft-drop algorithm [37] is used to identify the subjets of a high- $p_T$  W/Z/H boson candidate jet. This algorithm is applied to large-radius jets reclustered with the Cambridge–Aachen algorithm [38, 39], using an angular exponent  $\beta = 0$  and a soft-cutoff threshold  $z_{\text{cut}} < 0.1$ , which removes soft, wide-angle radiation from the jet. Neural-network-based taggers calibrated using collision data [34, 36, 40, 41] are used to assign each large-radius jet to one of the following classes: a single quark or gluon, a W or Z boson decaying to  $q\bar{q}$ , an H or Z boson decaying to  $b\bar{b}$  or  $c\bar{c}$ , and a top quark decaying hadronically.

The missing transverse momentum vector  $\vec{p}_T^{\text{miss}}$  is computed as the negative vector sum of the PUPPI-weighted transverse momenta of all the PF candidates in an event; its magnitude is denoted as  $p_T^{\text{miss}}$  [32]. The  $\vec{p}_T^{\text{miss}}$  is modified to account for corrections to the energy scale of the reconstructed jets in the event. Anomalous high- $p_T^{\text{miss}}$  events can be due to a variety of reconstruction failures, detector malfunctions or noncollision backgrounds. Such events are rejected by event filters that are designed to identify more than 85–90% of the spurious high- $p_T^{\text{miss}}$  events with a misidentification rate less than 0.1% [32].

### 3 Signal models and theoretical framework

Several theoretical models, including composite Higgs scenarios [17, 42, 43] and sequential extensions of the SM [44, 45], predict the existence of additional resonances with masses in the TeV range. The HVT framework [19] is based on an effective Lagrangian that provides a phenomenological description encompassing a broad class of these models.

The HVT framework introduces three new heavy bosons,  $W'^{\pm}$  and  $Z'$ , which are nearly degenerate in mass and have other properties analogous to those of the SM weak vector bosons. It allows for the exploration of a broad range of couplings between these heavy bosons and SM fermions and bosons. The relevant interaction Lagrangian is:

$$\mathcal{L}_{\mathcal{W}}^{\text{int}} = -g_q \mathcal{W}_\mu^a \bar{q}_k \gamma^\mu \frac{\sigma_a}{2} q_k - g_\ell \mathcal{W}_\mu^a \bar{l}_k \gamma^\mu \frac{\sigma_a}{2} l_k - g_H (\mathcal{W}_\mu^a \Phi^\dagger \frac{\sigma_a}{2} iD^\mu \Phi + \text{h.c.}), \quad (1)$$

where  $q_k$  and  $l_k$  denote the left-handed quark and lepton field doublets of generation  $k$  ( $k = 1, 2, 3$ );  $\Phi$  is the Higgs doublet;  $\sigma_a$  ( $a = 1, 2, 3$ ) are the Pauli matrices; and  $g_q$ ,  $g_\ell$ , and  $g_H$  represent the couplings of the heavy triplet field  $\mathcal{W}$  to SM quarks, leptons, and the Higgs boson, respectively. Right-handed fermions do not couple directly to  $\mathcal{W}$ . The fermion couplings  $g_q$

and  $g_\ell$  are assumed to be generation-universal, unless stated otherwise. The triplet also couples to the Higgs boson and, by the equivalence theorem, to longitudinally polarized W and Z bosons.

The interaction structure is defined by three main parameters:  $g_V$ , which sets the overall strength of the new interaction, and the dimensionless parameters  $c_H$  and  $c_F$ . The coupling to the Higgs and longitudinal vector bosons is given by  $g_H = g_V c_H$ , while the generation-universal coupling to fermions is given by  $g_F = g_q = g_\ell = g^2 c_F / g_V$ . Here,  $g = 2m_W/v \approx 0.65$ , where  $m_W$  is the W boson mass and  $v$  is the vacuum expectation value of the Higgs field [46].

Within this framework, three benchmark models are defined to represent different production and decay scenarios [19], referred to as models A, B, and C. Models A and B assume quark-antiquark annihilation via the DY process as the dominant production mechanism, while model C assumes production exclusively through VBF. The distinction between models A and B lies in the relative strengths of the couplings to bosons and fermions. Model A represents a weakly coupled extension of the SM based on an extended gauge symmetry [44]. In model A, the parameter values are set to  $g_H = -0.56$ ,  $g_F = -0.55$ , and  $g_V = 1$ . Model B corresponds to a strongly coupled scenario, as in composite Higgs models [17], with  $g_H = -2.93$ ,  $g_F = 0.15$ , and  $g_V = 3$ . Both model A and B parameter values are set to the explicit theory scenario described in Ref. [19]. In model B, the  $W'$  and  $Z'$  bosons have larger intrinsic widths than in model A, but these are still narrower than the experimental resolution in most channels included in the combination. Over the explored parameter space, the relative width  $\Gamma/m$  of the  $V'$  resonances remains below 5%. For decays to fermion pairs, model A yields larger branching fractions, with each lepton generation contributing about 4%, compared to approximately 0.2% in model B. Conversely, decays to VV or VH final states have branching fractions of about 2% in model A and nearly 50% in model B. Lastly, model C sets  $g_H = 1, 3, \text{ or } 6$  and  $g_V = 1$ , and assumes exclusive VBF production by setting  $g_F = 0$ , resulting in a  $V'$  boson that does not couple to SM fermions.

The production cross sections for the DY and VBF processes scale with the squares of the relevant couplings:

$$\sigma_{\text{DY}} = g_F^2 \hat{\sigma}_{\text{DY}}, \quad \sigma_{\text{VBF}} = g_H^2 \hat{\sigma}_{\text{VBF}}, \quad (2)$$

where  $\hat{\sigma}_{\text{DY}}$  and  $\hat{\sigma}_{\text{VBF}}$  are the reduced cross sections calculated with the coupling parameters factored out.

## 4 Input channels

The individual channels included in this statistical combination are briefly summarized in the following. For comprehensive descriptions, the reader is referred to the original publications listed in Table 1.

This combined statistical analysis targets heavy resonances with masses between 1 and 8 TeV. In this regime, the W, Z, and H bosons, as well as top quarks produced in  $V'$  boson decays, typically have a high Lorentz boost in the laboratory frame. When these bosons decay hadronically, their decay products are often collimated and reconstructed as single large-radius jets, which are identified using jet substructure and machine-learning-based algorithms. In most searches, the resonance mass is reconstructed from a pair of such large-radius jets. Exceptions include channels, such as  $W' \rightarrow WZ$  [57] and  $Z' \rightarrow t\bar{t}$  ( $1\ell$ ) [54], where hadronic reconstructed candidates are also resolved as multiple small-radius jets, and channels  $W' \rightarrow \ell\bar{\nu}$  [49],  $W' \rightarrow \tau\bar{\nu}$  [50],  $Z' \rightarrow ZH$  [55, 56], and  $W' \rightarrow WZ$  [58], where the presence of neutrinos from the Z boson decay prevents full mass reconstruction, and the transverse mass is used instead. Several channels of

Table 1: Summary of the searches for dfermion and diboson resonances used as inputs to this combined statistical analysis. The targeted production modes, resonance mass ranges, reconstructed particles, and references are listed. In the “Jets” column, only jets from the heavy resonance decay are indicated. Detailed definitions of reconstructed particles in the “Leptons” and “Jets” columns, such as  $\tau_h$  and various types of jets, are provided later in the main text.

Channel	Prod. modes	$m_{V'}$ range [TeV]	Leptons	Jets	Reference
$Z' \rightarrow \tau^+ \tau^-$	DY	0.5–4.0	$\ell \tau_h$ or $2\tau_h$	—	[47]
$Z' \rightarrow \ell^+ \ell^-$	DY	0.8–5.5	$2\ell$	—	[48]
$W' \rightarrow \ell \bar{\nu}$	DY	0.8–6.0	$1\ell$	—	[49]
$W' \rightarrow \tau \bar{\nu}$	DY	0.8–6.0	$1\tau_h$	—	[50]
$V' \rightarrow q\bar{q}^{(\prime)}$	DY	1.8–8.7	$0\ell$	$jj$	[51]
$W' \rightarrow t\bar{b}$ (0 $\ell$ )	DY	1.0–4.0	$0\ell$	$j^t j^b$	[52]
$W' \rightarrow t\bar{b}$ (1 $\ell$ )	DY	2.0–6.0	$1\ell$	$j^b j^b$	[53]
$Z' \rightarrow t\bar{t}$ (1 $\ell$ )	DY	0.8–5.0	$1\ell$	$j^t$ or $jjj^b$	[54]
$Z' \rightarrow ZH$ (2 $\ell$ 2b)	DY + VBF	0.8–5.0	$2\ell$	$j^{bb}$	[55]
$Z' \rightarrow ZH$ (2 $\nu$ 2b)	DY + VBF	0.8–5.0	$0\ell$	$j^{bb}$	[55]
$Z' \rightarrow ZH$ (2 $\ell$ 2q)	DY	1.2–6.0	$2\ell$	$j^H$	[56]
$Z' \rightarrow ZH$ (2 $\nu$ 2q)	DY	1.2–6.0	$0\ell$	$j^H$	[56]
$W' \rightarrow WZ$ (2q2 $\ell$ )	DY	0.6–2.0	$2\ell$	$j^V$ or $jj$	[57]
$W' \rightarrow WZ$ (2q2 $\nu$ )	DY + VBF	1.0–4.5	$0\ell$	$j^V$	[58]
$V' \rightarrow WV/WH$	DY + VBF	1.0–4.5	$1\ell$	$j^V$	[59]
$V' \rightarrow VV/VH$	DY + VBF	1.3–6.0	$0\ell$	$j^V j^V$	[20]

diboson final states further enhance sensitivity to the VBF production mode by selecting events with two additional small-radius jets that have a large invariant mass and a large separation in pseudorapidity.

The analysis channels are categorized according to the reconstructed final-state candidates:

- $\ell$ : muons or electrons,
- $\tau_h$ : hadronically decaying  $\tau$  leptons,
- $j$ : small-radius jets,
- $j^b$ : small-radius jets identified as originating from b quarks (b-tagged),
- $j^V$ : large-radius jets identified as W or Z bosons decaying to  $q\bar{q}$  (V tagged),
- $j^{bb}$ : large-radius jets identified as H or Z bosons decaying to  $b\bar{b}$  (double-b tagged),
- $j^H$ : large-radius jets identified as H bosons decaying hadronically (H tagged), and
- $j^t$ : large-radius jets identified as hadronically decaying top quarks (t tagged).

In all channels, the signal is searched for as a localized excess over a smoothly falling background in the reconstructed mass or transverse mass spectrum. Background estimation strategies vary by channel. Analyses involving leptons and small-radius jets primarily rely on Monte Carlo (MC) simulations to model the background. In contrast, analyses that use neural-network-based, large-radius jet taggers employ control samples in data to estimate the background, as the misidentification rates for these taggers are challenging to simulate accurately.

To ensure statistical independence among channels, event selections were designed to avoid overlaps in both the signal and control regions. Mutual exclusivity is enforced in most chan-

---

nels through requirements on lepton and jet multiplicities. If overlaps are identified, the overlapping events are retained in the combination only in the channel that provides the highest expected sensitivity for a given signal model and mass hypothesis.

In channels targeting fermionic decays of  $V'$  bosons, overlaps primarily occur among fully hadronic final states. The inclusive dijet search  $V' \rightarrow q\bar{q}^{(\prime)}$  [51], which requires only two high- $p_T$  jets, overlaps with all other fully hadronic channels because of its inclusive event selection and is therefore excluded whenever a more sensitive channel covers the same phase space. Two additional searches for  $Z' \rightarrow b\bar{b}$  [60] and  $Z' \rightarrow t\bar{t} (0\ell)$  [61] are not included in this combination because they have a large overlap with the inclusive  $V' \rightarrow q\bar{q}^{(\prime)}$  search [51]. These channels are specifically optimized to study exclusive final states. They provide enhanced sensitivity relative to the inclusive  $V' \rightarrow q\bar{q}^{(\prime)}$  search for BSM scenarios other than the one probed in this combination. Overlaps also occur in channels with one lepton, such as  $W' \rightarrow t\bar{b}$  [53] and  $Z' \rightarrow t\bar{t}$  [54], where one of the top quarks decays leptonically.

In the diboson channels, each channel requires either at least two high- $p_T$  small-radius jets or a single large-radius jet consistent with a hadronically decaying boson. Event categories are constructed to be mutually exclusive using selections based on lepton and jet multiplicities, as well as the invariant mass of final-state candidates. In the  $Z' \rightarrow ZH$  [55] channel, events are categorized based on the number of b-tagged subjets within the large-radius jet, defining a 2-b-tag and a  $\leq 1$ -b-tag categories. The latter category overlaps with the signal region of the  $Z' \rightarrow ZH$  [56] channel and is not included in the combination, as the other channel is more sensitive in this phase space. In addition, the  $W' \rightarrow WZ$  [57] channel uses a 2-b-tag category as a control region, which overlaps with the signal region of the  $Z' \rightarrow ZH$  [55] channel. To maintain statistical independence, the b-tagged categories of the  $W' \rightarrow WZ$  [57] channel are therefore excluded from the combination.

## 5 Systematic uncertainties

An overview of the main experimental and theoretical systematic uncertainties considered in the analyses included in the combination is provided in the following. Detailed descriptions can be found in the original publications listed in Table 1. The sensitivity of the combined analysis is limited by the statistical uncertainty, with all systematic uncertainties being subdominant. A summary of the main systematic uncertainties is presented in Table 2.

Theoretical uncertainties arise from variations in the renormalization and factorization scales used in the matrix element calculations, as well as from the choice of the parton distribution functions (PDFs) and their internal parameters. The PDF uncertainties are evaluated with either the NNPDF3.0 [62] or NNPDF3.1 [63] sets, depending on the analysis. Uncertainties from scale variations are treated as correlated across all analyses. The PDF uncertainties are treated as correlated among analyses that use the same PDF set and as uncorrelated otherwise. The impact of these theoretical uncertainties is separated into the acceptance and normalization effects. In analyses where the acceptance uncertainty for the signal was found to be negligible, it is not included. The normalization components of these uncertainties for the signal are included in the theoretical cross section predictions for each model, following the prescription of Ref. [19].

Most analyses rely on simulation to model background processes, incorporating theoretical uncertainties from PDFs and from scale variations. Minor backgrounds, such as single top quark and diboson processes, are typically subdominant and are assigned inclusive cross section uncertainties. The treatment of subdominant backgrounds varies across analyses and is

Table 2: Summary of the main systematic uncertainties. The second column specifies whether the uncertainty affects the yield (Y), the shape (Sh) of the distributions, or both. The “Effects” columns summarize the typical impact of the uncertainty on the yield, migration, and signal shape parameters. Analyses are split by fermion and boson signatures. The letters “S”, “B”, and “SB” indicate whether the uncertainty affects the signal, the dominant background, or both, respectively. The letter “U” denotes cases where background parameters are unconstrained or allowed to float freely in the fit. A dash “—” refers to cases where an uncertainty has a negligible effect or is not applicable.

	Type	Effects	$Z' \rightarrow \tau^+ \tau^-$ [47]	$Z' \rightarrow \ell^+ \ell^-$ [48]	$W' \rightarrow \ell \bar{\nu}$ [49]	$W' \rightarrow \tau \bar{\tau}$ [50]	$V' \rightarrow q \bar{q}^{(\prime)}$ [51]	$W' \rightarrow b \bar{b}$ [52]	$W' \rightarrow t \bar{b}$ [53]	$Z' \rightarrow t \bar{t}$ [54]	Effects	$Z' \rightarrow Z H$ [55]	$Z' \rightarrow Z H$ [56]	$W' \rightarrow W Z$ [57]	$W' \rightarrow W Z$ [58]	$V' \rightarrow V V/W H$ [59]	$V' \rightarrow V V/V H$ [20]
Sig. PDF and scale	Y, Sh	2–20%	S	—	—	S	—	S	—	S	0.3–30%	S	S	S	S	S	S
Bkg. PDF and scale	Y, Sh	2–50%	B	—	B	B	—	B	B	B	0.1–20%	B	—	—	B	—	—
Bkg. modeling	Y, Sh	1–100%	B	U	B	B	U	B	B	B	4–50%	U	U	B	B	B	B
Jet energy scale/res.	Y, Sh	1–40%	—	—	SB	SB	S	SB	SB	SB	0.2–35%	SB	S	SB	SB	S	SB
Jet mass scale/res.	Y, Sh	2–5%	—	—	—	—	—	—	—	—	0.3–2.6%	SB	—	SB	SB	SB	S
H tagging	Y	—	—	—	—	—	—	—	—	—	0.4–15%	S	S	—	—	S	SB
V tagging	Y	—	—	—	—	—	—	—	—	—	1.2–33%	—	—	SB	SB	S	SB
t tagging	Y, Sh	21–36%	—	—	—	—	—	—	SB	—	1–3%	—	—	—	—	—	B
b tagging and veto	Y, Sh	1–23%	SB	—	—	—	—	SB	SB	SB	0.1–15%	SB	S	SB	SB	S	—
e, $\mu$ id., iso., trigger	Y, Sh	0.5–8%	SB	S	SB	SB	—	—	SB	SB	0.9–7%	SB	S	SB	—	SB	—
e, $\mu$ energy scale/res.	Y, Sh	1–6%	S	S	SB	SB	—	—	SB	—	0.1–3%	S	—	SB	—	S	—
$\tau_h$ reco., id., iso.	Y	5–10%	S	—	—	SB	—	—	—	—	—	—	—	—	—	—	—
$\tau_h$ energy scale/res.	Y, Sh	1.5–5%	S	—	—	SB	—	—	—	—	—	—	—	—	—	—	—
Int. luminosity	Y	1.2–2.5%	SB	S	SB	SB	S	SB	SB	SB	1.2–2.5%	SB	S	SB	SB	S	SB
$p_T^{\text{miss}}$ scale	Y, Sh	2–5%	—	—	SB	SB	—	—	—	—	0.1–2.4%	SB	—	—	SB	S	—
Pileup	Y, Sh	0.6–5%	—	—	SB	SB	—	SB	SB	SB	0.1–4%	SB	S	SB	SB	S	SB
L1 trigger inefficiency	Y, Sh	0.5–5%	—	—	SB	SB	—	SB	—	—	0.2–1%	—	S	SB	SB	—	SB

not detailed here. The modeling of the QCD multijet background also differs between analyses. For instance, in the  $V' \rightarrow q \bar{q}^{(\prime)}$  analysis, this background is predicted from the data by fitting the dijet invariant mass distribution, while in the fully hadronic diboson channels, it is estimated using simulation. Because of differences in phase space definitions and normalization strategies, background-related uncertainties are generally treated as uncorrelated across analyses, even when originating from the same underlying physics process.

Jet-related systematic uncertainties play a critical role in analyses involving hadronic or lepton+jets final states, where precise jet reconstruction and flavor tagging are essential for signal identification and background suppression. For small-radius jets, the dominant sources of uncertainty include variations in the jet energy scale and resolution. For large-radius jets, uncertainties in the jet energy and mass scales, as well as their respective resolutions, are particularly important. These uncertainties are propagated to both signal and background processes and are treated as correlated across analyses that use the same jet type. Jet-tagging uncertainties, including those for H, V, b, and t tagging, are derived from measurements of tagging efficiencies and misidentification rates. Uncertainties associated with the same tagging algorithm and calibration strategy are treated as correlated across analyses.

For electrons and muons, systematic uncertainties arise from the energy or momentum scale and resolution measurements, as well as from the reconstruction, trigger, and identification efficiencies. These uncertainties are typically correlated between signal and background, and

also across the analyses that use the same lepton selection criteria. Lepton-related uncertainties are particularly important in the  $W' \rightarrow \ell\bar{\nu}$  and  $Z' \rightarrow \ell^+\ell^-$  analyses, as detector resolution and energy scale calibration significantly impact the modeling of the  $W \rightarrow \ell\bar{\nu}$  and  $Z \rightarrow \ell^+\ell^-$  backgrounds.

Additional systematic uncertainties arise from the energy scale of unclustered particles contributing to  $p_T^{\text{miss}}$ , the integrated luminosity, pileup modeling, and the inefficiency of the L1 trigger due to detector timing drift [25]. The uncertainties in the integrated luminosity for the 2016, 2017, and 2018 data-taking periods range from 1.2 to 2.5% [64–66], with a combined uncertainty of 1.6% for the full data set.

## 6 Results and interpretation

The combined results are obtained through a simultaneous maximum likelihood fit across the individual analyses using the CMS statistical analysis tool COMBINE [67], which is based on the ROOFIT [68] and ROOSTATS [69] frameworks. In each individual channel, the data are found to be globally in agreement with the expectations from the SM. A goodness-of-fit test of the combined analysis, based on a saturated test statistic [70], yields a  $p$ -value of approximately 34% under the background-only hypothesis. This result indicates that the data are compatible with the SM prediction.

The observed and expected 95% confidence level (CL) upper limits on the signal production cross section and other parameters of interest (POIs) are computed using a modified frequentist CL<sub>s</sub> method [71, 72], with an asymptotic approximation [73]. This approach uses a profile likelihood ratio test statistic where systematic uncertainties are modeled as nuisance parameters [67]. The POIs include the signal strength ( $\mu$ ), defined as the ratio of the measured product of cross section and branching fraction ( $\sigma\mathcal{B}$ ) to its theoretical expectation, and the coupling strength parameters ( $g_F$ ,  $g_V$ ,  $g_H$ ). Upper limits on the production cross section or couplings strengths are derived as functions of the resonance mass. The evolution of the expected signal shape, acceptance, and branching fraction with the mass hypothesis is fully incorporated into the statistical model.

In certain channels, the asymptotic approximation becomes inaccurate in low-yield regimes, particularly in the high-mass tails of the reconstructed mass distributions. In these cases, MC pseudo-experiments are performed to validate the accuracy of the asymptotic method, with nuisance parameters related to systematic uncertainties fixed to their post-fit values. For the  $Z' \rightarrow \ell^+\ell^-$  and  $W' \rightarrow \ell\bar{\nu}$  channels in the high-mass regime (above 4 TeV), the asymptotic approximation is found to overestimate the sensitivity by approximately 15% compared to the results obtained from MC pseudo-experiments. This discrepancy is negligible in all other channels.

Figures 2 and 3 present the expected and observed 95% CL upper limits on the  $V'$  boson production cross section as functions of the resonance mass  $m_{V'}$  for the individual analyses targeting hadronic, leptonic, and bosonic final states, as well as for their combination. The analyses are categorized according to the  $V'$  boson decay mode, denoted as  $V' \rightarrow \text{quarks}$ ,  $V' \rightarrow \text{leptons}$ , and  $V' \rightarrow \text{bosons}$ . The limits for the  $V' \rightarrow \text{quarks}$  and  $V' \rightarrow \text{leptons}$  categories are evaluated under the HVT model A scenario, while the  $V' \rightarrow \text{bosons}$  limits assume model B. The dominant sensitivity in the  $V' \rightarrow \text{quarks}$  category arises from the fully hadronic  $W' \rightarrow t\bar{b}$  channel for resonance masses below 2 TeV and from the  $V' \rightarrow q\bar{q}^{(\prime)}$  channel at higher masses. In the  $V' \rightarrow \text{leptons}$  category, the leading contributions come from the  $W' \rightarrow \ell\bar{\nu}$  and  $Z' \rightarrow \ell^+\ell^-$  channels across the entire mass range. For  $V' \rightarrow \text{bosons}$  category, the sensitivity is primarily

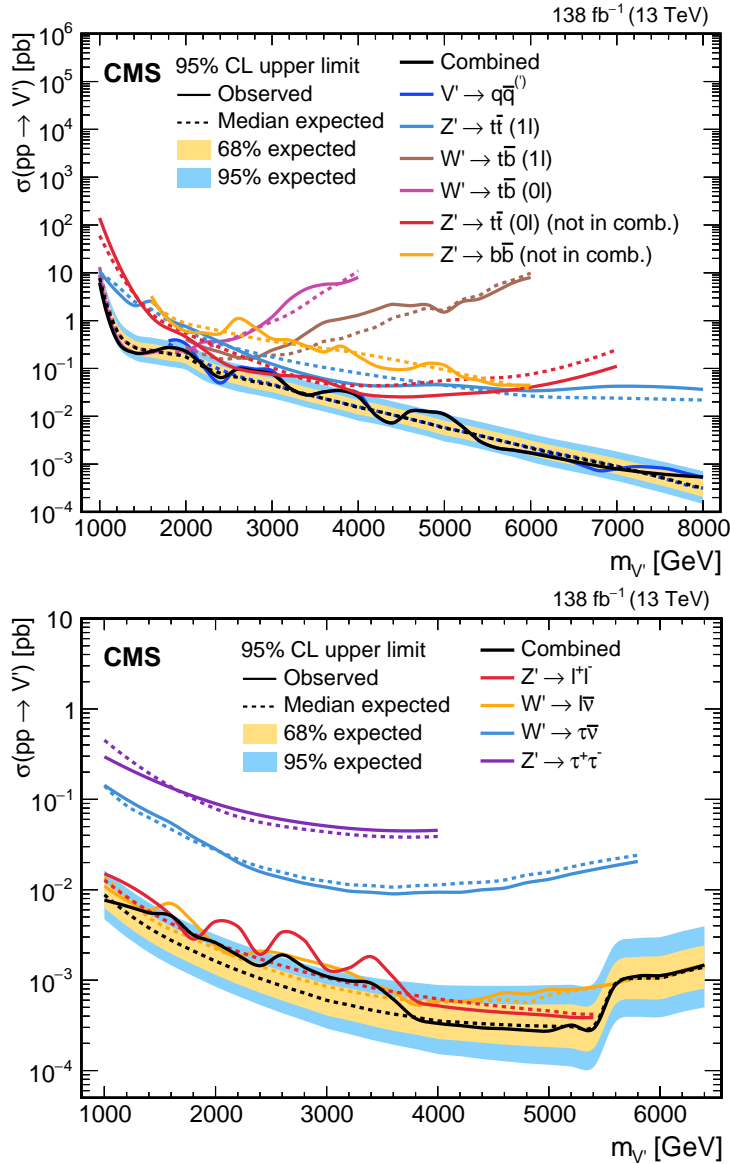


Figure 2: Expected and observed 95% CL upper limits on the  $V'$  boson production cross section as functions of the resonance mass  $m_{V'}$  shown separately for the  $V' \rightarrow$  quarks (upper) and  $V' \rightarrow$  leptons (lower) categories. The limits are evaluated in the HVT model A scenario.

driven by the fully hadronic  $VV$  and  $VH$  channels.

Figures 4 and 5 show the combined limits from all contributing channels for each HVT model. For model A, the dominant contribution from leptonic channels excludes  $V'$  resonances with masses below 5.5 TeV. Above this mass, the sensitivity of the  $Z' \rightarrow \ell^+\ell^-$  channel is statistically limited, and the combined limit is driven by the  $W' \rightarrow \ell\bar{\nu}$  channel. For model B, the bosonic channels dominate the sensitivity, excluding masses below 4.8 TeV. In model C, where only bosonic decays contribute, masses between 1.2 and 1.4 TeV are excluded for  $g_H = 3$ , and masses below 2 TeV are excluded for  $g_H = 6$ . A decomposition of the combined limits into the individual  $W'$  and  $Z'$  contributions is provided in Appendix A.

No significant excess above the SM expectation is observed in the combined analysis. The most significant local excesses in individual channels, those with a local significance greater than 2 SD, were not consistent across channels, leading to a reduction of their significance in

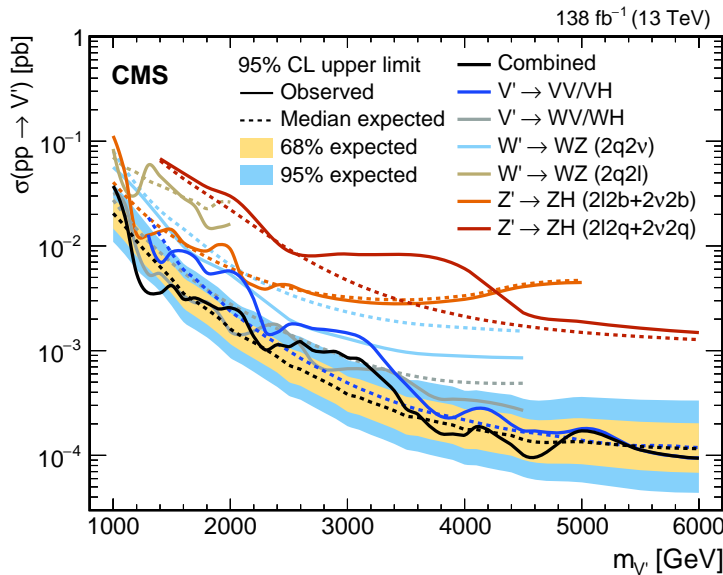


Figure 3: Expected and observed 95% CL upper limits on the  $V'$  boson production cross section as functions of the resonance mass  $m_{V'}$  shown separately for the  $V' \rightarrow$  bosons category. The limits are evaluated under the HVT model B scenario.

the combined result. The largest excesses observed in model A have local significances of 2.4 SD and 2.1 SD at masses of 2.6 and 3.4 TeV, respectively. These excesses are primarily driven by the  $Z' \rightarrow \ell^+ \ell^-$  channel, and their significance is reduced compared to the previous CMS result [48]. For model B, the largest excesses have a local significance of 2.3 SD at 2.9 TeV and 2.4 SD at 3.0 TeV, dominated by the  $V' \rightarrow$  bosons categories. This combination also reduces the local significance of the previously reported CMS excesses of 3.6 SD at 2.1 and 2.9 TeV [20]. The largest excess in model C, with a local significance of 2.8 SD at a mass of 1 TeV, is also reduced in the combination, with the main contribution from the WV and WH final state, as compared to the previous CMS result [59]. The combination does not confirm the excess of events over the background prediction previously reported by the ATLAS Collaboration in the region around 1.5 TeV [11].

Overall, this combination sets the most stringent limits to date for HVT models B and C. The improved sensitivity is primarily driven by the fully hadronic final states [20], which benefit from the use of advanced jet substructure tagging techniques and a three-dimensional signal extraction strategy. The combined limits in model A, whose sensitivity is instead dominated by the leptonic channels, are comparable with those obtained by the ATLAS Collaboration [11].

Additionally, exclusion limits are set in the HVT  $g_F$ - $g_H$  coupling parameter space for representative resonance masses of 3 and 4 TeV, with  $\mu$  and  $g_V$  fixed to 1. The 3 and 4 TeV mass points are chosen as commonly used HVT benchmark values, enabling direct comparison with previous CMS and other LHC results. The expected and observed 95% CL upper limits are shown in Figs. 6 and 7, with results presented separately for the  $V' \rightarrow$  quarks,  $V' \rightarrow$  leptons, and  $V' \rightarrow$  bosons categories, as well as for their combination. The same qualitative conclusions discussed for Figs. 2 and 3 hold here. The  $V' \rightarrow$  quarks category is dominated by the fully hadronic  $V' \rightarrow q\bar{q}^{(\prime)}$  channel, the  $V' \rightarrow$  leptons category by the  $W' \rightarrow \ell\bar{\nu}$  and  $Z' \rightarrow \ell^+ \ell^-$  channels, and the  $V' \rightarrow$  bosons category by the fully hadronic VV and VH final states. The sensitivity to the couplings is complementary across the channels. At large values of  $g_H$ , the sensitivity is primarily driven by the  $V' \rightarrow$  bosons category, while the  $V' \rightarrow$  leptons categories dominate at small  $g_H$  values. The full combination results for the  $g_F$ - $g_H$  plane for resonance

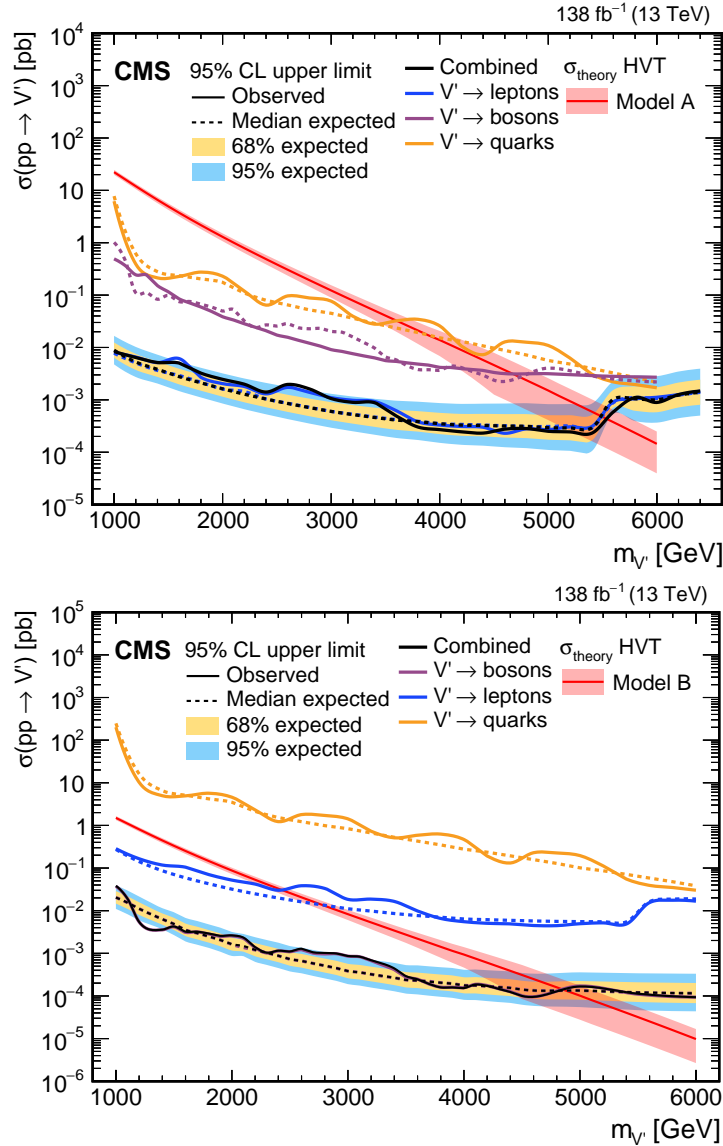


Figure 4: Expected and observed 95% CL upper limits on the  $V'$  boson production cross section as functions of the resonance mass  $m_{V'}$  in the HVT models A (upper) and B (lower). The line corresponding to the  $V' \rightarrow$  bosons category almost entirely overlaps with the combined result in the lower plot.

masses of 3 and 4 TeV are shown in Fig. 7. Compared to previous results with 2016 data alone, the constraint on  $g_F$  is improved by a factor of 1.9 to 2.6, depending on the resonance mass and the value of  $g_H$ .

To explore scenarios beyond the assumption of fermion universality, the coupling strength  $g_F$  is split into four distinct components:  $g_{q_{12}}$  for light quarks,  $g_{q_3}$  for third-generation quarks,  $g_{\ell_{12}}$  for light leptons, and  $g_{\ell_3}$  for third-generation leptons. Together with  $\mu$ ,  $g_V$ , and  $g_H$ , this extension totals seven POIs in the HVT framework. For this study, the signal strength  $\mu$  and the overall coupling  $g_V$  are fixed to 1, leaving five POIs. We focus on two-dimensional parameter scans involving  $g_{q_3}$ , since the largest sensitivity gains are observed in channels with third-generation quarks, such as  $t\bar{t}$  and  $t\bar{b}$ . This leads to three key coupling planes:  $g_{q_3}$ - $g_{q_{12}}$ ,  $g_{q_3}$ - $g_{\ell_3}$ , and  $g_{q_3}$ - $g_H$ .

In the first case, exclusion limits are evaluated in the  $g_{q_3}$ - $g_{q_{12}}$  plane, with  $g_{\ell_{12}}$ ,  $g_{\ell_3}$ , and  $g_H$  set to

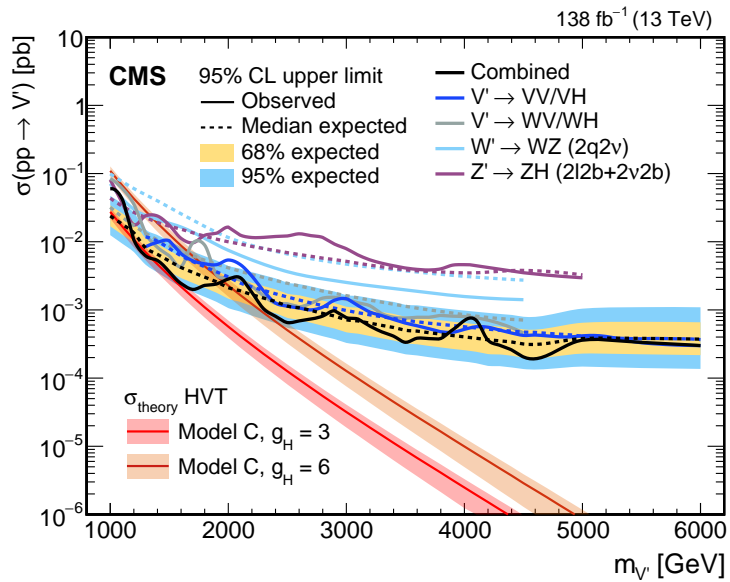


Figure 5: Expected and observed 95% CL upper limits on the  $V'$  boson production cross section as functions of the resonance mass  $m_{V'}$  in the HVT model C.

zero. This probes the possibility of nonuniversal couplings between light and third-generation quarks. In this plane, the most sensitive channels are the  $Z' \rightarrow t\bar{t}$  channel at large  $g_{q_3}$  values and the  $V' \rightarrow q\bar{q}'$  channel at large  $g_{q_{12}}$  values, as shown in Fig. 8.

Additional scans are performed in the  $g_{q_3}$ - $g_{\ell_3}$  and  $g_{q_3}$ - $g_H$  planes, this time fixing the remaining couplings to their HVT model A values. Here, setting all other couplings to zero is not viable; for instance, setting  $g_{q_{12}} = 0$  would eliminate DY production entirely. The resulting parameter regions are fully excluded at 95% CL, driven by the combined sensitivity of  $V' \rightarrow$  quarks,  $V' \rightarrow$  leptons, and  $V' \rightarrow$  bosons categories. The complementarity of the individual channels allows for the complete exclusion of these parameter spaces, which could not be achieved by any single channel alone.

## 7 Summary

A combined statistical analysis of searches for heavy vector boson resonances decaying into pairs of  $W$ ,  $Z$ , or  $H$  bosons, as well as into quark pairs ( $q\bar{q}$ ,  $b\bar{b}$ ,  $t\bar{t}$ , or  $t\bar{b}$ ) or lepton pairs ( $\ell^+\ell^-$ ,  $\ell\bar{\nu}$ ), with  $\ell = e, \mu, \tau$ , has been presented. The results are based on proton-proton collision data at a center-of-mass energy of 13 TeV, corresponding to an integrated luminosity of  $138 \text{ fb}^{-1}$ , collected by the CMS experiment from 2016 to 2018. No significant deviation from the expectations of the standard model is observed. The results are interpreted in the simplified heavy vector triplet framework, setting 95% confidence level upper limits on the production cross sections of heavy vector bosons. These limits are further interpreted as constraints on their couplings to standard model particles. The results exclude heavy vector boson resonances with a mass below 5.5 TeV in a weakly coupled scenario, below 4.8 TeV in a strongly coupled scenario, and up to 2.0 TeV in the case of production via vector boson fusion. These results represent a significant improvement over previous constraints, driven by the inclusion of a larger data set and advances in the underlying analyses. Compared to results with the 2016 data alone, the sensitivity is improved by a factor of 1.7 to 3.6 for the strongly coupled scenario and 4.4 to 7.7 for the weakly coupled scenario. This combination provides the most stringent and comprehensive constraints to date on the production of heavy vector triplet resonances.

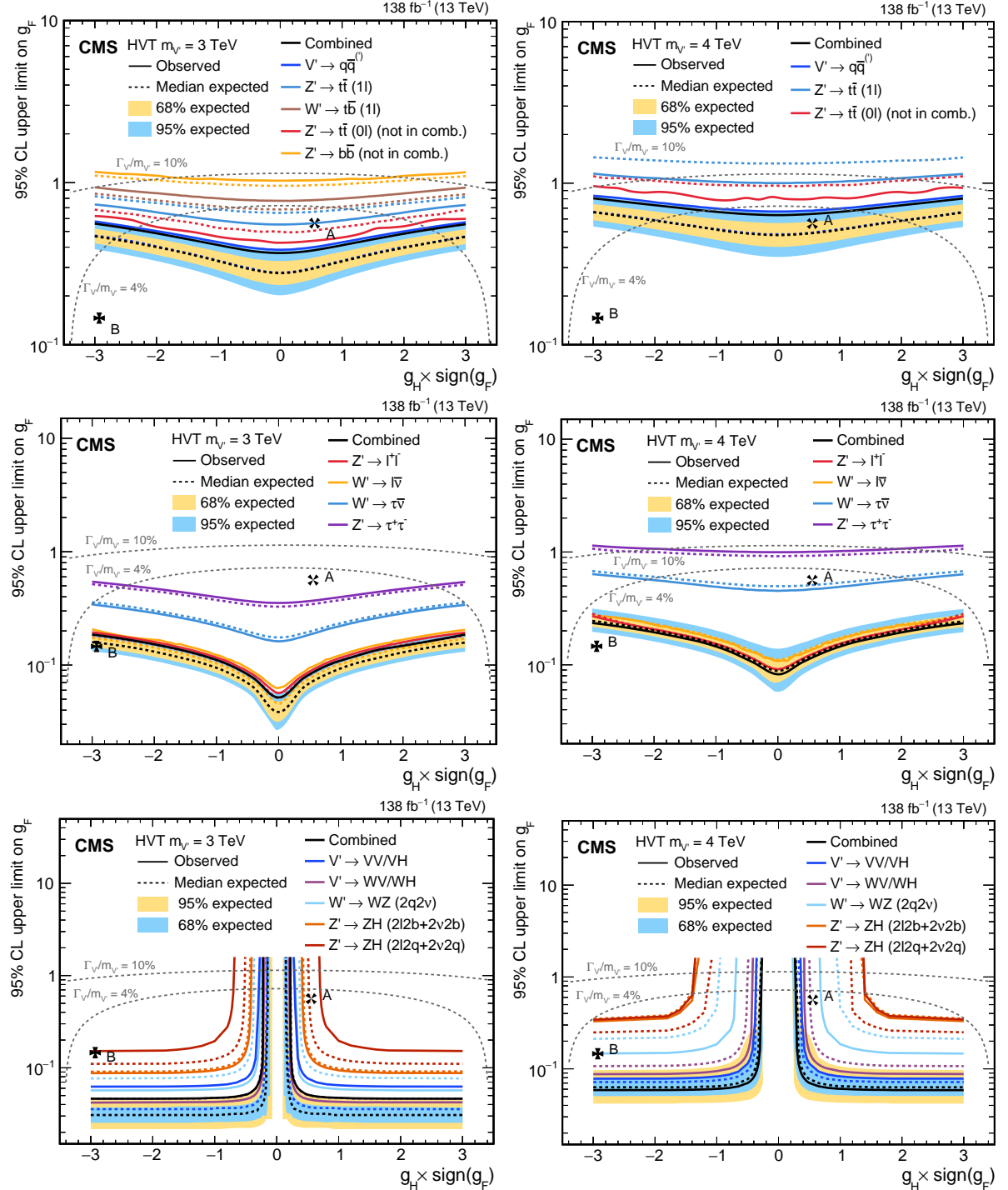


Figure 6: Expected and observed 95% CL upper limits on the coupling parameter  $g_F$  as functions of  $g_H$ , under the assumption  $g_V = 1$ . The results are shown separately for the  $V' \rightarrow$  quarks (upper),  $V' \rightarrow$  leptons (middle), and  $V' \rightarrow$  bosons (lower) categories for resonance masses of 3 TeV (left) and 4 TeV (right). The results from the individual channels are also shown. The gray dotted lines denote coupling values above which the relative width of the resonance,  $\Gamma_{V'}/m_{V'}$ , exceeds 4 and 10%. The couplings corresponding to the HVT models A and B are indicated by crosses.

## Acknowledgments

We congratulate our colleagues in the CERN accelerator departments for the excellent performance of the LHC and thank the technical and administrative staffs at CERN and at other CMS

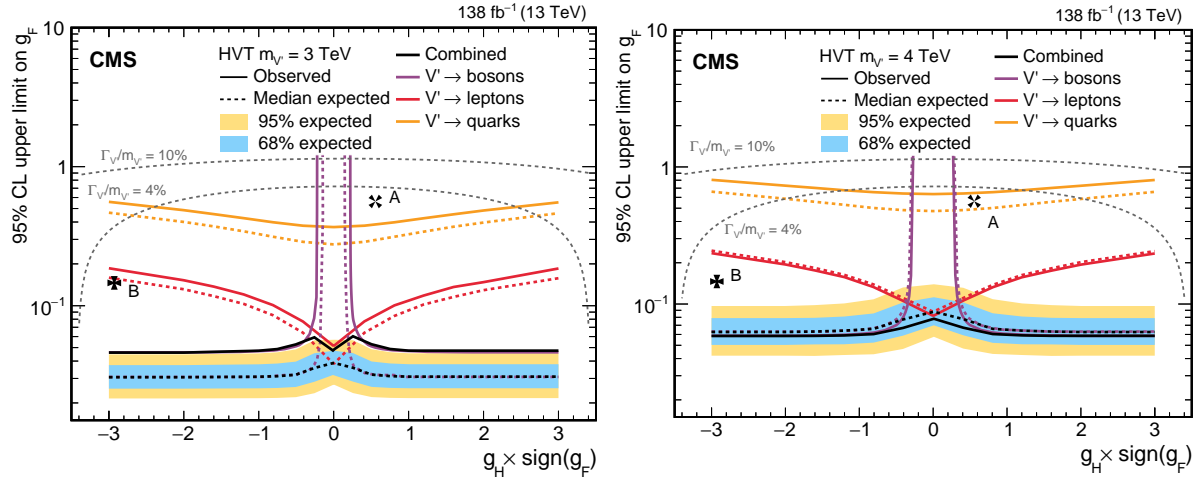


Figure 7: Expected and observed 95% CL upper limits on the coupling parameter  $g_F$  as functions of  $g_H$ , under the assumption  $g_V = 1$ . The combined results from all channels are shown for resonance masses of 3 TeV (left) and 4 TeV (right). The results from the individual channels are also shown. The gray dotted lines denote coupling values above which the relative width of the resonance,  $\Gamma_{V'}/m_{V'}$ , exceeds 4 and 10%. The couplings corresponding to the HVT models A and B are indicated by crosses.

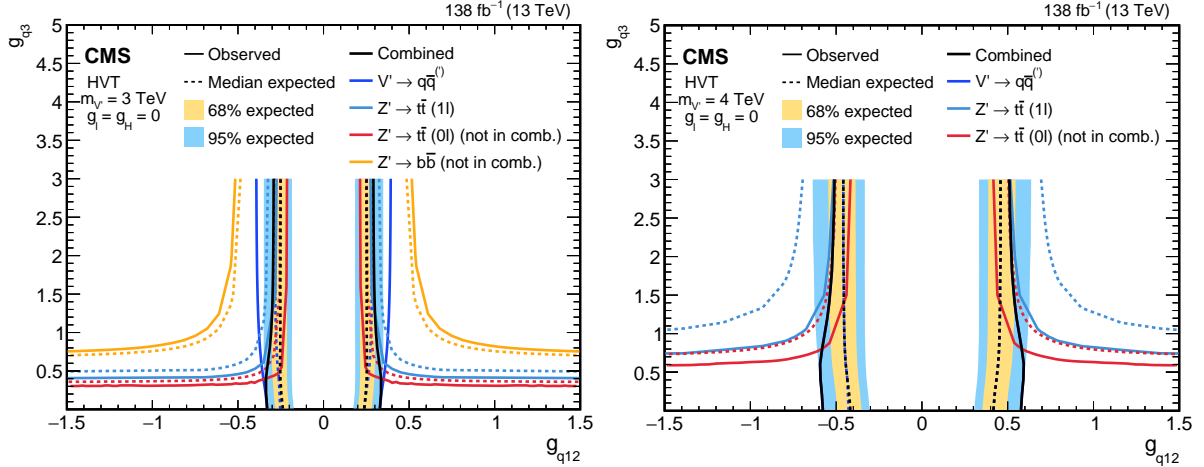


Figure 8: Expected and observed 95% CL upper limits on the coupling parameter  $g_{q_{12}}$  as functions of  $g_{q_3}$ , under the assumption  $g_V = 1$ ,  $g_{\ell_{12}} = 0$ ,  $g_{\ell_3} = 0$ , and  $g_H = 0$ . The results are shown for the  $V' \rightarrow$  quarks category for resonance masses of 3 TeV (left) and 4 TeV (right). The contributions from individual channels are also shown. The line corresponding to the  $V' \rightarrow q\bar{q}^{(\prime)}$  channel almost entirely overlaps with the combined result in the right plot. Regions with large absolute values of  $g_{q_{12}}$  are excluded for any value of  $g_{q_3}$ .

institutes for their contributions to the success of the CMS effort. In addition, we gratefully acknowledge the computing centers and personnel of the Worldwide LHC Computing Grid and other centers for delivering so effectively the computing infrastructure essential to our analyses. Finally, we acknowledge the enduring support for the construction and operation of the LHC, the CMS detector, and the supporting computing infrastructure provided by the following funding agencies: SC (Armenia), BMBWF and FWF (Austria); FNRS and FWO (Belgium); CNPq, CAPES, FAPERJ, FAPERGS, and FAPESP (Brazil); MES and BNSF (Bulgaria); CERN; CAS, MoST, and NSFC (China); MINCIENCIAS (Colombia); MSES and CSF (Croatia); RIF (Cyprus); SENESCYT (Ecuador); ERC PRG, TARISTU24-TK10 and MoER TK202 (Esto-

nia); Academy of Finland, MEC, and HIP (Finland); CEA and CNRS/IN2P3 (France); SRNSF (Georgia); BMFTR, DFG, and HGF (Germany); GSRI (Greece); NKFIH (Hungary); DAE and DST (India); IPM (Iran); SFI (Ireland); INFN (Italy); MSIT and NRF (Republic of Korea); MES (Latvia); LMTLT (Lithuania); MOE and UM (Malaysia); BUAP, CINVESTAV, CONACYT, LNS, SEP, and UASLP-FAI (Mexico); MOS (Montenegro); MBIE (New Zealand); PAEC (Pakistan); MES, NSC, and NAWA (Poland); FCT (Portugal); MESTD (Serbia); MICIU/AEI and PCTI (Spain); MOSTR (Sri Lanka); Swiss Funding Agencies (Switzerland); MST (Taipei); MHESI (Thailand); TUBITAK and TENMAK (Türkiye); NASU (Ukraine); STFC (United Kingdom); DOE and NSF (USA).

Individuals have received support from the Marie-Curie program and the European Research Council and Horizon 2020 Grant, contract Nos. 675440, 724704, 752730, 758316, 765710, 824093, 101115353, 101002207, 101001205, and COST Action CA16108 (European Union); the Leventis Foundation; the Alfred P. Sloan Foundation; the Alexander von Humboldt Foundation; the Science Committee, project no. 22rl-037 (Armenia); the Fonds pour la Formation à la Recherche dans l'Industrie et dans l'Agriculture (FRIA) and Fonds voor Wetenschappelijk Onderzoek contract No. 1228724N (Belgium); the Beijing Municipal Science & Technology Commission, No. Z191100007219010, the Fundamental Research Funds for the Central Universities, the Ministry of Science and Technology of China under Grant No. 2023YFA1605804, the Natural Science Foundation of China under Grant No. 12535004, and USTC Research Funds of the Double First-Class Initiative No. YD2030002017 (China); the Ministry of Education, Youth and Sports (MEYS) of the Czech Republic; the Shota Rustaveli National Science Foundation, grant FR-22-985 (Georgia); the Deutsche Forschungsgemeinschaft (DFG), among others, under Germany's Excellence Strategy – EXC 2121 "Quantum Universe" – 390833306, and under project number 400140256 - GRK2497; the Hellenic Foundation for Research and Innovation (HFRI), Project Number 2288 (Greece); the Hungarian Academy of Sciences, the New National Excellence Program - ÚNKP, the NKFIH research grants K 131991, K 133046, K 138136, K 143460, K 143477, K 146913, K 146914, K 147048, 2020-2.2.1-ED-2021-00181, TKP2021-NKTA-64, and 2025-1.1.5-NEMZ\_KI-2025-00004 (Hungary); the Council of Science and Industrial Research, India; ICSC – National Research Center for High Performance Computing, Big Data and Quantum Computing, FAIR – Future Artificial Intelligence Research, and CUP I53D23001070006 (Mission 4 Component 1), funded by the NextGenerationEU program (Italy); the Latvian Council of Science; the Ministry of Education and Science, project no. 2022/WK/14, and the National Science Center, contracts Opus 2021/41/B/ST2/01369, 2021/43/B/ST2/01552, 2023/49/B/ST2/03273, and the NAWA contract BPN/PPO/2021/1/00011 (Poland); the Fundação para a Ciência e a Tecnologia, grant CEECIND/01334/2018 (Portugal); the National Priorities Research Program by Qatar National Research Fund; MICIU/AEI/10.13039/501100011033, ERDF/EU, "European Union NextGenerationEU/PRTR", and Programa Severo Ochoa del Principado de Asturias (Spain); the Chulalongkorn Academic into Its 2nd Century Project Advancement Project, the National Science, Research and Innovation Fund program IND\_FF\_68\_369\_2300\_097, and the Program Management Unit for Human Resources & Institutional Development, Research and Innovation, grant B39G680009 (Thailand); the Kavli Foundation; the Nvidia Corporation; the SuperMicro Corporation; the Welch Foundation, contract C-1845; and the Weston Havens Foundation (USA).

## References

- [1] UA1 Collaboration, "Experimental observation of isolated large transverse energy electrons with associated missing energy at  $\sqrt{s} = 540 \text{ GeV}$ ", *Phys. Lett. B* **122** (1983) 103, doi:10.1016/0370-2693(83)91177-2.

[2] UA2 Collaboration, “Observation of single isolated electrons of high transverse momentum in events with missing transverse energy at the CERN  $\bar{p}p$  collider”, *Phys. Lett. B* **122** (1983) 476, doi:10.1016/0370-2693(83)91605-2.

[3] UA1 Collaboration, “Experimental observation of lepton pairs of invariant mass around  $95\text{ GeV}/c^2$  at the CERN SPS collider”, *Phys. Lett. B* **126** (1983) 398, doi:10.1016/0370-2693(83)90188-0.

[4] UA2 Collaboration, “Evidence for  $Z^0 \rightarrow e^+e^-$  at the CERN  $\bar{p}p$  collider”, *Phys. Lett. B* **129** (1983) 130, doi:10.1016/0370-2693(83)90744-X.

[5] ATLAS Collaboration, “Observation of a new particle in the search for the standard model Higgs boson with the ATLAS detector at the LHC”, *Phys. Lett. B* **716** (2012) 1, doi:10.1016/j.physletb.2012.08.020, arXiv:1207.7214.

[6] CMS Collaboration, “Observation of a new boson at a mass of 125 GeV with the CMS experiment at the LHC”, *Phys. Lett. B* **716** (2012) 30, doi:10.1016/j.physletb.2012.08.021, arXiv:1207.7235.

[7] CMS Collaboration, “Observation of a new boson with mass near 125 GeV in  $pp$  collisions at  $\sqrt{s} = 7$  and 8 TeV”, *JHEP* **06** (2013) 081, doi:10.1007/JHEP06(2013)081, arXiv:1303.4571.

[8] F. del Aguila, J. de Blas, and M. Perez-Victoria, “Electroweak limits on general new vector bosons”, *JHEP* **09** (2010) 033, doi:10.1007/JHEP09(2010)033, arXiv:1005.3998.

[9] J. de Blas, J. M. Lizana, and M. Perez-Victoria, “Combining searches of  $Z'$  and  $W'$  bosons”, *JHEP* **01** (2013) 166, doi:10.1007/JHEP01(2013)166, arXiv:1211.2229.

[10] CMS Collaboration, “Combination of CMS searches for heavy resonances decaying to pairs of bosons or leptons”, *Phys. Lett. B* **798** (2019) 134952, doi:10.1016/j.physletb.2019.134952, arXiv:1906.00057.

[11] ATLAS Collaboration, “Combination of searches for heavy spin-1 resonances using 139  $\text{fb}^{-1}$  of proton-proton collision data at  $\sqrt{s} = 13$  TeV with the ATLAS detector”, *JHEP* **04** (2024) 118, doi:10.1007/JHEP04(2024)118, arXiv:2402.10607.

[12] CMS Collaboration, “Searches for Higgs boson production through decays of heavy resonances”, *Phys. Rept.* **1115** (2025) 368, doi:10.1016/j.physrep.2024.09.004, arXiv:2403.16926.

[13] E. Salvioni, G. Villadoro, and F. Zwirner, “Minimal  $Z'$  models: Present bounds and early LHC reach”, *JHEP* **11** (2009) 068, doi:10.1088/1126-6708/2009/11/068, arXiv:0909.1320.

[14] M. Schmaltz and C. Spethmann, “Two simple  $W'$  models for the early LHC”, *JHEP* **07** (2011) 046, doi:10.1007/jhep07(2011)046, arXiv:1011.5918.

[15] M. Schmaltz and D. Tucker-Smith, “Little Higgs review”, *Ann. Rev. Nucl. Part. Sci.* **55** (2005) 229, doi:10.1146/annurev.nucl.55.090704.151502, arXiv:hep-ph/0502182.

[16] M. Perelstein, “Little Higgs models and their phenomenology”, *Prog. Part. Nucl. Phys.* **58** (2007) 247, doi:10.1016/j.ppnp.2006.04.001, arXiv:hep-ph/0512128.

- [17] R. Contino, D. Marzocca, D. Pappadopulo, and R. Rattazzi, “On the effect of resonances in composite Higgs phenomenology”, *JHEP* **10** (2011) 081, doi:10.1007/JHEP10(2011)081, arXiv:1109.1570.
- [18] D. Abercrombie et al., “Dark matter benchmark models for early LHC Run 2 searches: Report of the ATLAS/CMS dark matter forum”, *Phys. Dark Univ.* **27** (2020) 100371, doi:10.1016/j.dark.2019.100371, arXiv:1507.00966.
- [19] D. Pappadopulo, A. Thamm, R. Torre, and A. Wulzer, “Heavy vector triplets: Bridging theory and data”, *JHEP* **09** (2014) 060, doi:10.1007/JHEP09(2014)060, arXiv:1402.4431.
- [20] CMS Collaboration, “Search for new heavy resonances decaying to WW, WZ, ZZ, WH, or ZH boson pairs in the all-jets final state in proton-proton collisions at  $\sqrt{s} = 13$  TeV”, *Phys. Lett. B* **844** (2023) 137813, doi:10.1016/j.physletb.2023.137813, arXiv:2210.00043.
- [21] “HEPData record for this analysis”, 2025. doi:10.17182/hepdata.166217.
- [22] CMS Collaboration, “The CMS experiment at the CERN LHC”, *JINST* **3** (2008) S08004, doi:10.1088/1748-0221/3/08/S08004.
- [23] CMS Collaboration, “Development of the CMS detector for the CERN LHC Run 3”, *JINST* **19** (2024) P05064, doi:10.1088/1748-0221/19/05/P05064, arXiv:2309.05466.
- [24] CMS Collaboration, “The CMS trigger system”, *JINST* **12** (2017) P01020, doi:10.1088/1748-0221/12/01/P01020, arXiv:1609.02366.
- [25] CMS Collaboration, “Performance of the CMS Level-1 trigger in proton–proton collisions at  $\sqrt{s} = 13$  TeV”, *JINST* **15** (2020) P10017, doi:10.1088/1748-0221/15/10/P10017, arXiv:2006.10165.
- [26] CMS Collaboration, “Performance of the CMS high-level trigger during LHC Run 2”, *JINST* **19** (2024) P11021, doi:10.1088/1748-0221/19/11/P11021, arXiv:2410.17038.
- [27] CMS Collaboration, “Particle-flow reconstruction and global event description with the CMS detector”, *JINST* **12** (2017) P10003, doi:10.1088/1748-0221/12/10/P10003, arXiv:1706.04965.
- [28] M. Cacciari, G. P. Salam, and G. Soyez, “The anti- $k_T$  jet clustering algorithm”, *JHEP* **04** (2008) 063, doi:10.1088/1126-6708/2008/04/063, arXiv:0802.1189.
- [29] M. Cacciari, G. P. Salam, and G. Soyez, “FastJet user manual”, *Eur. Phys. J. C* **72** (2012) 1896, doi:10.1140/epjc/s10052-012-1896-2, arXiv:1111.6097.
- [30] D. Bertolini, P. Harris, M. Low, and N. Tran, “Pileup per particle identification”, *JHEP* **10** (2014) 059, doi:10.1007/JHEP10(2014)059, arXiv:1407.6013.
- [31] CMS Collaboration, “Pileup mitigation at CMS in 13 TeV data”, *JINST* **15** (2020) P09018, doi:10.1088/1748-0221/15/09/p09018, arXiv:2003.00503.
- [32] CMS Collaboration, “Performance of missing transverse momentum reconstruction in proton-proton collisions at  $\sqrt{s} = 13$  TeV using the CMS detector”, *JINST* **14** (2019) P07004, doi:10.1088/1748-0221/14/07/P07004, arXiv:1903.06078.

- [33] CMS Collaboration, “Jet energy scale and resolution in the CMS experiment in pp collisions at 8 TeV”, *JINST* **12** (2017) P02014, doi:10.1088/1748-0221/12/02/P02014, arXiv:1607.03663.
- [34] CMS Collaboration, “Identification of heavy-flavour jets with the CMS detector in pp collisions at 13 TeV”, *JINST* **13** (2018) P05011, doi:10.1088/1748-0221/13/05/P05011, arXiv:1712.07158.
- [35] E. Bols et al., “Jet flavour classification using DeepJet”, *JINST* **15** (2020) P12012, doi:10.1088/1748-0221/15/12/P12012, arXiv:2008.10519.
- [36] CMS Collaboration, “Performance of heavy-flavour jet identification in Lorentz-boosted topologies in proton-proton collisions at  $\sqrt{s} = 13$  TeV”, *JINST* **20** (2025) P11006, doi:10.1088/1748-0221/20/11/P11006, arXiv:2510.10228.
- [37] A. J. Larkoski, S. Marzani, G. Soyez, and J. Thaler, “Soft drop”, *JHEP* **05** (2014) 146, doi:10.1007/JHEP05(2014)146, arXiv:1402.2657.
- [38] Y. L. Dokshitzer, G. D. Leder, S. Moretti, and B. R. Webber, “Better jet clustering algorithms”, *JHEP* **08** (1997) 001, doi:10.1088/1126-6708/1997/08/001, arXiv:hep-ph/9707323.
- [39] M. Wobisch and T. Wengler, “Hadronization corrections to jet cross-sections in deep inelastic scattering”, in *Proc. of the Workshop on Monte Carlo Generators for HERA Physics, Hamburg, Germany*. 1998. arXiv:hep-ph/9907280.
- [40] CMS Collaboration, “Identification of heavy, energetic, hadronically decaying particles using machine-learning techniques”, *JINST* **15** (2020) P06005, doi:10.1088/1748-0221/15/06/P06005, arXiv:2004.08262.
- [41] H. Qu and L. Gouskos, “ParticleNet: Jet tagging via particle clouds”, *Phys. Rev. D* **101** (2020) 056019, doi:10.1103/PhysRevD.101.056019, arXiv:1902.08570.
- [42] E. Accomando et al., “Charged di-boson production at the LHC in a 4-site model with a composite Higgs boson”, *Phys. Rev. D* **86** (2012) 115006, doi:10.1103/PhysRevD.86.115006, arXiv:1208.0268.
- [43] B. Bellazzini, C. Csáki, and J. Serra, “Composite Higgses”, *Eur. Phys. J. C* **74** (2014) 2766, doi:10.1140/epjc/s10052-014-2766-x, arXiv:1401.2457.
- [44] V. D. Barger, W.-Y. Keung, and E. Ma, “A gauge model with light W and Z bosons”, *Phys. Rev. D* **22** (1980) 727, doi:10.1103/PhysRevD.22.727.
- [45] C. Grojean, E. Salvioni, and R. Torre, “A weakly constrained W’ at the early LHC”, *JHEP* **07** (2011) 002, doi:10.1007/JHEP07(2011)002, arXiv:1103.2761.
- [46] Particle Data Group, S. Navas et al., “Review of particle physics”, *Phys. Rev. D* **110** (2024) 030001, doi:10.1103/PhysRevD.110.030001.
- [47] CMS Collaboration, “Search for heavy neutral resonances decaying to tau lepton pairs in proton-proton collisions at  $\sqrt{s} = 13$  TeV”, *Phys. Rev. D* **111** (2025) 112004, doi:10.1103/PhysRevD.111.112004, arXiv:2412.04357.
- [48] CMS Collaboration, “Search for resonant and nonresonant new phenomena in high-mass dilepton final states at  $\sqrt{s} = 13$  TeV”, *JHEP* **07** (2021) 208, doi:10.1007/JHEP07(2021)208, arXiv:2103.02708.

[49] CMS Collaboration, “Search for new physics in the lepton plus missing transverse momentum final state in proton-proton collisions at  $\sqrt{s} = 13$  TeV”, *JHEP* **07** (2022) 067, doi:10.1007/JHEP07(2022)067, arXiv:2202.06075.

[50] CMS Collaboration, “Search for new physics in the  $\tau$  lepton plus missing transverse momentum final state in proton-proton collisions at  $\sqrt{s} = 13$  TeV”, *JHEP* **09** (2023) 051, doi:10.1007/JHEP09(2023)051, arXiv:2212.12604.

[51] CMS Collaboration, “Search for high mass dijet resonances with a new background prediction method in proton-proton collisions at  $\sqrt{s} = 13$  TeV”, *JHEP* **05** (2020) 033, doi:10.1007/JHEP05(2020)033, arXiv:1911.03947.

[52] CMS Collaboration, “Search for  $W'$  bosons decaying to a top and a bottom quark at  $\sqrt{s} = 13$  TeV in the hadronic final state”, *Phys. Lett. B* **820** (2021) 136535, doi:10.1016/j.physletb.2021.136535, arXiv:2104.04831.

[53] CMS Collaboration, “Search for  $W'$  bosons decaying to a top and a bottom quark in leptonic final states in proton-proton collisions at  $\sqrt{s} = 13$  TeV”, *JHEP* **05** (2024) 046, doi:10.1007/JHEP05(2024)046, arXiv:2310.19893.

[54] CMS Collaboration, “Search for new particles decaying into top quark-antiquark pairs in events with one lepton and jets in proton-proton collisions at 13 TeV”, CMS Physics Analysis Summary CMS-PAS-B2G-22-006, 2025.

[55] CMS Collaboration, “Search for a heavy vector resonance decaying to a  $Z$  boson and a Higgs boson in proton-proton collisions at  $\sqrt{s} = 13$  TeV”, *Eur. Phys. J. C* **81** (2021) 688, doi:10.1140/epjc/s10052-021-09348-6, arXiv:2102.08198.

[56] CMS Collaboration, “Search for a heavy resonance decaying into a  $Z$  and a Higgs boson in events with an energetic jet and two electrons, two muons, or missing transverse momentum in proton-proton collisions at  $\sqrt{s} = 13$  TeV”, *JHEP* **02** (2025) 089, doi:10.1007/JHEP02(2025)089, arXiv:2411.00202.

[57] CMS Collaboration, “Search for heavy resonances decaying to  $ZZ$  or  $ZW$  and axion-like particles mediating nonresonant  $ZZ$  or  $ZH$  production at  $\sqrt{s} = 13$  TeV”, *JHEP* **04** (2022) 087, doi:10.1007/JHEP04(2022)087, arXiv:2111.13669.

[58] CMS Collaboration, “Search for heavy resonances decaying to  $Z(\nu\bar{\nu})V(q\bar{q}')$  in proton-proton collisions at  $\sqrt{s} = 13$  TeV”, *Phys. Rev. D* **106** (2022) 012004, doi:10.1103/PhysRevD.106.012004, arXiv:2109.08268.

[59] CMS Collaboration, “Search for heavy resonances decaying to  $WW$ ,  $WZ$ , or  $WH$  boson pairs in the lepton plus merged jet final state in proton-proton collisions at  $\sqrt{s} = 13$  TeV”, *Phys. Rev. D* **105** (2022) 032008, doi:10.1103/PhysRevD.105.032008, arXiv:2109.06055.

[60] CMS Collaboration, “Search for narrow resonances in the  $b$ -tagged dijet mass spectrum in proton-proton collisions at  $\sqrt{s} = 13$  TeV”, *Phys. Rev. D* **108** (2023) 012009, doi:10.1103/PhysRevD.108.012009, arXiv:2205.01835.

[61] CMS Collaboration, “Search for  $t\bar{t}$  resonances in the fully hadronic final state”, CMS Physics Analysis Summary CMS-PAS-B2G-24-003, 2025.

[62] NNPDF Collaboration, “Parton distributions for the LHC Run II”, *JHEP* **04** (2015) 040, doi:10.1007/JHEP04(2015)040, arXiv:1410.8849.

- [63] NNPDF Collaboration, “Parton distributions from high-precision collider data”, *Eur. Phys. J. C* **77** (2017) 663, doi:10.1140/epjc/s10052-017-5199-5, arXiv:1706.00428.
- [64] CMS Collaboration, “Precision luminosity measurement in proton-proton collisions at  $\sqrt{s} = 13$  TeV in 2015 and 2016 at CMS”, *Eur. Phys. J. C* **81** (2021) 800, doi:10.1140/epjc/s10052-021-09538-2, arXiv:2104.01927.
- [65] CMS Collaboration, “CMS luminosity measurement for the 2017 data-taking period at  $\sqrt{s} = 13$  TeV”, CMS Physics Analysis Summary CMS-PAS-LUM-17-004, 2018.
- [66] CMS Collaboration, “CMS luminosity measurement for the 2018 data-taking period at  $\sqrt{s} = 13$  TeV”, CMS Physics Analysis Summary CMS-PAS-LUM-18-002, 2019.
- [67] CMS Collaboration, “The CMS Statistical Analysis and Combination Tool: COMBINE”, *Comput. Softw. Big Sci.* **8** (2024) 19, doi:10.1007/s41781-024-00121-4, arXiv:2404.06614.
- [68] W. Verkerke and D. Kirkby, “The ROOFIT toolkit for data modeling”, in *Proc. 13th Int. Conf. on Computing in High Energy and Nuclear Physics (CHEP 2003): La Jolla CA, United States, March 24–28. 2003*. arXiv:physics/0306116.
- [69] L. Moneta et al., “The ROOSTATS project”, in *Proc. 13th Int. Workshop on Advanced Computing and Analysis Techniques in Physics Research (ACAT 2010): Jaipur, India, February 22–27. 2010*. arXiv:1009.1003. doi:10.22323/1.093.0057.
- [70] R. D. Cousins, “Lectures on statistics in theory: Prelude to statistics in practice”, 2018. arXiv:1807.05996.
- [71] T. Junk, “Confidence level computation for combining searches with small statistics”, *Nucl. Instrum. Meth. A* **434** (1999) 435, doi:10.1016/S0168-9002(99)00498-2, arXiv:hep-ex/9902006.
- [72] A. L. Read, “Presentation of search results: The  $CL_s$  technique”, *J. Phys. G* **28** (2002) 2693, doi:10.1088/0954-3899/28/10/313.
- [73] G. Cowan, K. Cranmer, E. Gross, and O. Vitells, “Asymptotic formulae for likelihood-based tests of new physics”, *Eur. Phys. J. C* **71** (2011) 1554, doi:10.1140/epjc/s10052-011-1554-0, arXiv:1007.1727. [Erratum: doi:10.1140/epjc/s10052-013-2501-z].

## A Additional figures

A breakdown of the exclusion limits by  $W'$  and  $Z'$  combinations under the three HVT benchmark models is shown in Figs. A.1 and A.2.

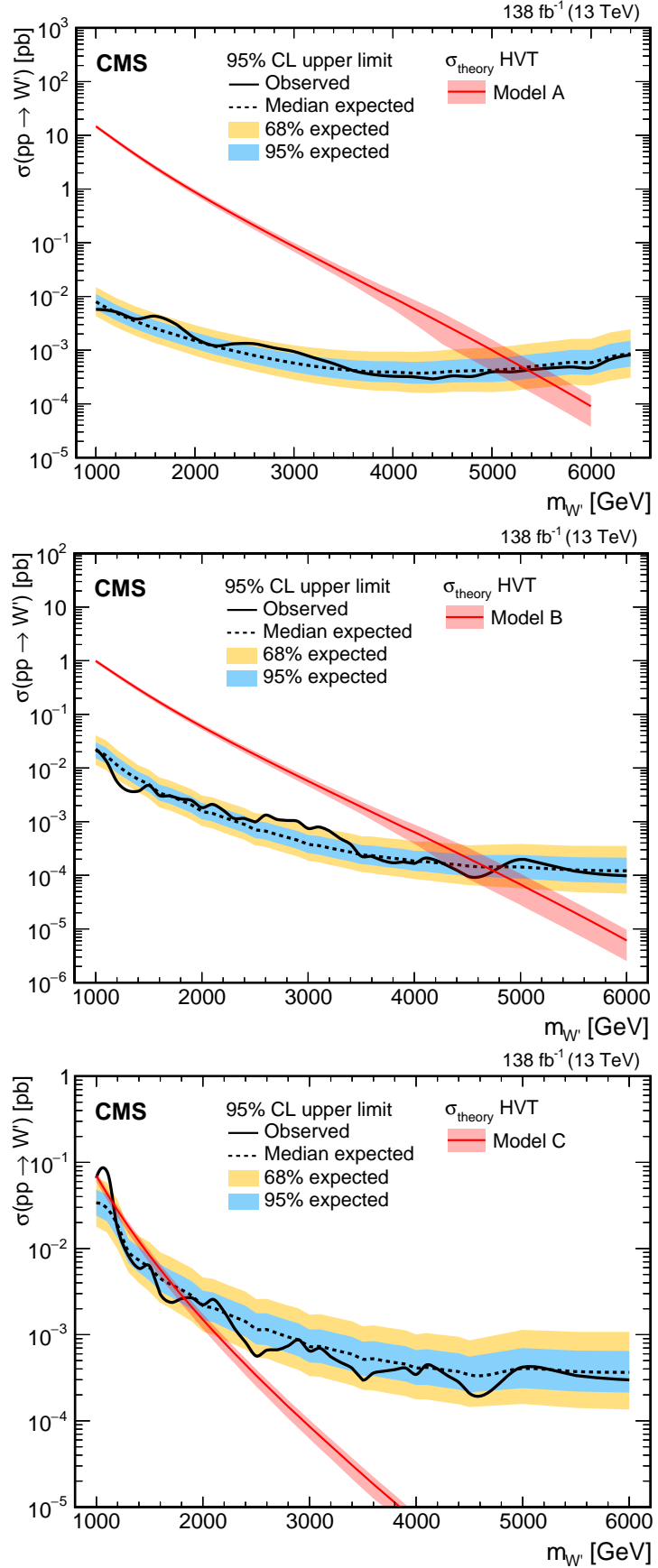


Figure A.1: Expected and observed 95% CL upper limits on the  $W'$  boson production cross section as a function of the resonance mass  $m_{W'}$  for the  $W'$  interpretations. The limits are evaluated in the HVT model A (upper), B (middle), and C (lower) scenarios.

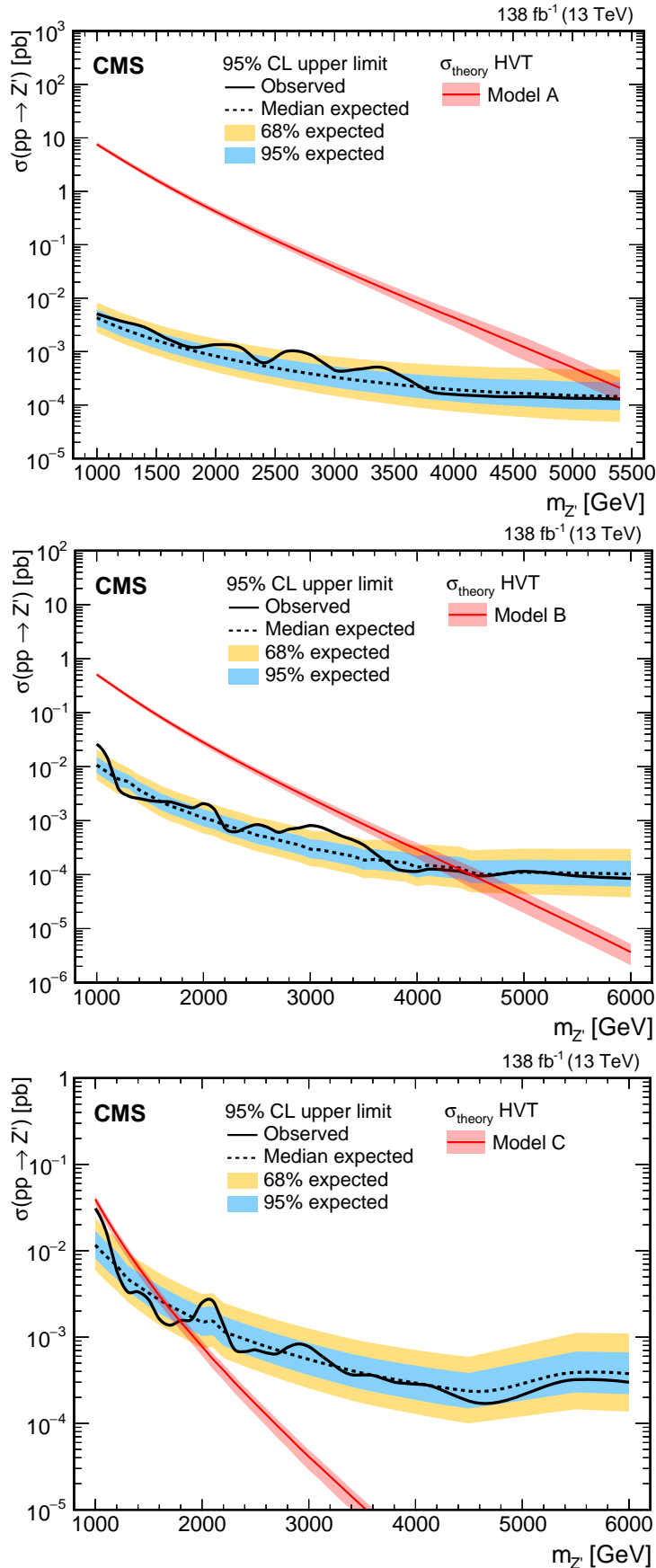


Figure A.2: Expected and observed 95% CL upper limits on the  $Z'$  boson production cross section as a function of the resonance mass  $m_{Z'}$  for the  $Z'$  interpretations. The limits are evaluated in the HVT model A (upper), B (middle), and C (lower) scenarios.